

The Event-specific Geomorphological Instantaneous Unit Hydrograph (E-GIUH): The basin hydrological response characteristic of a flood event

Hervé Andrieu¹, Roger Moussa², Pierre-Emmanuel Kirstetter^{3,4,5,6}

¹ GERS-LEE, Univ. Gustave Eiffel, IFSTTAR, F-44344 Bouguenais, France

² LISAH, Univ. Montpellier, INRAE, IRD, Montpellier SupAgro, Montpellier, France

³ School of Civil Engineering and Environmental Science, University of Oklahoma, Norman, OK 73072, USA

⁴ School of Meteorology, University of Oklahoma, Norman, OK 73072, USA

⁵ Advanced Radar Research Center, University of Oklahoma, Norman OK 73072, USA

⁶ NOAA / National Severe Storms Laboratory, Norman OK 73072, USA

Submitted for publication in the Journal of Hydrology

Corresponding author: Hervé Andrieu, AndrieuHerve@orange.fr

Keywords : GIUH, Flash-flood, rainfall-runoff modeling, Inverse method, Rainfall spatial variability

Highlights:

- The Width Function-GIUH has been modified to project the spatial distribution of rainfall onto the hydrological network.

- By accounting for the influence of rainfall on the hydrological response of catchments, an Event specific - GIUH (E-GIUH) is defined for each flood event.

- The identification of an E-GIUH from observed data (hydrograph and rain field time series) is treated as an inverse problem.

- The proposed identification method is applied to a sample of flooding events on two catchments within the OHMCV Observatory territory, in confirming the wide diversity of E-GIUHs.

- A sensitivity analysis indicates that the method is fairly robust and easy to use, which is most encouraging for large-scale applications.

30
31
32
33
34
35
36
37
38
39
40
41
42
43
44
45
46
47

Abstract:

In the field of hydrology, the Geomorphological Instantaneous Unit Hydrograph (GIUH) is central to describing a watershed response. The application of GIUH is extended to individual hydrological events by accounting for the influence of rainfall spatial distribution. A method is proposed herein to identify the Geomorphological Instantaneous Unit Hydrograph specific to each flood event (i.e. E-GIUH), when runoff of effective rainfall is the dominant process. The E-GIUH is derived from observational data, namely: rainfall field time series, and a hydrograph. Such an identification process is formulated as an inverse problem with parameters such as the E-GIUH velocity and coefficient of dispersion, as well as the hyetograph of rainfall excess. The proposed method is applied to several flood events across two mountainous catchments within the Cevennes-Vivarais Mediterranean Hydrometeorological Observatory territory prone to flash flooding. Results indicate that the E-GIUHs display significant variability over the two basins, and the E-GIUH parameters appear to be correlated with the flood event magnitude. The E-GIUH synthesizes the basin response to rain forcing and can be considered as a signature of flood events. A sensitivity study suggests that E-GIUH identification is fairly robust, even with respect to the *a priori* hyetograph of effective rainfall.

48 **1. Introduction**

49

50 The concept of the Geomorphological Instantaneous Unit Hydrograph (GIUH), defined as the probability
51 density function (pdf) of water travel time along the channel links of the hydrographic network, was developed
52 by (Gupta et al., 1980; Rodriguez-Iturbe and Valdés, 1979) by linking the unit hydrograph (Dooge, 1959;
53 Sherman, L.K., 1932) to the geomorphological parameters of a catchment. The emergence of GIUH has
54 contributed to the success of lumped rainfall-runoff models, which are widely used for their parsimony and
55 robustness in both flash flood prediction and hydrograph analysis when runoff of effective rainfall is the
56 dominant process of floods (Wood et al., 1990) . More specifically, the GIUH is well suited to treating the
57 ungauged basin modeling problem, which pertains to the longstanding challenge of regional modeling over large
58 areas, as exposed in the review paper by (Singh et al., 2014). The widespread use of GIUH within the hydrology
59 community coupled with its development over the decades attests to its relevance in representing watershed
60 responses and moreover confirms the ability of this approach to complement distributed models (Fatichi et al.,
61 2016).

62

63 The initial GIUH formulation relies on the channel links in hydrographic networks, as described by the
64 Horton classification. (Marani et al., 1991) and (Rodriguez-Iturbe and Rinaldo, 1997) extended this formulation
65 to the probability density function (pdf) of hydrological distances to the basin outlet, as described by the Width
66 Function (Kirkby, 1976), and went on to propose the Width Function Geomorphological Approach (D’Odorico
67 and Rigon, 2003; Rigon et al., 2016). An assumption of constant velocity is adopted to convert the distribution of
68 flow distances into a pdf of travel times along flow paths. The travel time pdf may be represented by the
69 Advection Dispersion Equation (ADE) (Rinaldo et al., 1991) and a unique solution of the Diffusive Wave
70 Equation (Hayami, 1951; Moussa, 1997). The GIUH is thus defined by the Width Function and the two
71 parameters characterizing the ADE and DWE, i.e. flow velocity and coefficient of dispersion. (Saco and Kumar,
72 2002a) justified this constant velocity assumption by showing that varying flow path velocities can be taken into
73 account by means of a kinematic-geomorphic dispersion that increases the coefficient of dispersion parameter.

74

75 GIUH applications often rely on a unique set of parameters in order to calibrate the model (e.g. (Boudhraâ et
76 al., 2018; Chen et al., 2019; Choi et al., 2011; Moussa, 1997; Yao et al., 2014), thereby suggesting that a single
77 representative GIUH can be associated with a catchment. However, several studies have highlighted the
78 influence on the catchment response of: i) the rain spatial distribution (Emmanuel et al., 2017; Goni et al., 2019;

79 Olivera and Maidment, 1999; Zoccatelli et al., 2010), and ii) the rain event magnitude (Rodriguez et al., 2005;
80 Saco and Kumar, 2002b). These findings have been confirmed by the post-event analysis of floods, (Smith et al.,
81 2005, 2002) among others, and simulation studies (Emmanuel et al., 2015; Volpi et al., 2012), hence
82 acknowledging the GIUH limitations listed by (Rigon et al., 2016), who specifically noted these shortcomings
83 when accounting for the rainfall distribution. Broadly speaking, these results indicate that the GIUH depends on
84 rainfall-runoff processes that drive the flow dynamics in the hydrograph network. Consequently, every flood
85 event can be characterized by its own GIUH, hereafter denoted as the E-GIUH, which is capable of enriching the
86 signatures of hydrological processes driving the basin response to rainfall forcing at the flood event scale
87 (McMillan, 2020).

88

89 This manuscript aims to advance the width function-based GIUH by: i) adapting its formulation in order to
90 account for the influence of spatial rainfall variability, and ii) proposing a method to determine the E-GIUH for
91 each flood event. First, the GIUH formulation is adapted to take into account the spatial rainfall pattern by means
92 of replacing the width function by the rainfall width function (Emmanuel et al., 2015; Woods and Sivapalan,
93 1999). This improvement serves to overcome a key limitation of the GIUH, as highlighted by (Rigon et al.,
94 2016). Second, a novel E-GIUH identification method based on observed data is developed and tested. The
95 typical approach consists of assuming a production function and jointly calibrating the GIUH and the production
96 function parameters; hence, results depend on the *a priori* production function. To address this problem, the
97 original method proposed herein formulates Event-GIUH identification as an inverse problem (Menke, 2012;
98 Tarentola, A., 2005). Inverse theory was defined by (Menke, 2012) as “a set of mathematical techniques for
99 reducing data to obtain knowledge about the physical world on the basis of inferences drawn from observations”.

100 Inverse techniques have been used in hydrology, e.g. by (Pan and Wood, 2013) to derive spatially distributed
101 runoff, by (Fisher et al., 2020) for the purpose of determining spatially distributed continuous river discharge
102 from discrete flow data, as well as by (Boudhraâ et al., 2018) to derive the hyetograph of effective rainfall from
103 flow data. The E-GIUH is identified from the observed hydrograph and from an estimation of the hyetograph of
104 effective rainfall. It is likely that this hyetograph influences the resulting E-GIUH. The use of an inverse
105 algorithm makes it possible to explicitly consider the specific role of this hyetograph. It can be done by
106 considering it as a set of parameters of the problem to solve. The algorithm is initialized by the priori
107 information about this hyetograph which combines the estimation of the a-posteriori hyetograph and its
108 accuracy. The inverse algorithm will give more or less importance to the a priori hyetograph according to its
109 accuracy, and will propose an improved shape. More generally, the adopted framework is well adapted to

110 considering the weight of data, a priori parameter values and model on the solution based on their accuracy. The
 111 proposed approach extends the domain of application of the GIUH. It allows to characterize each event in terms
 112 of a specific E-GIUH that can be viewed as the signature of this event”.

113

114 Section 2 presents an adaptation of the width function-based GIUH, which takes into account the spatial
 115 rainfall variability and develops the approach employed to identify the E-GIUH from observed data, namely the
 116 hydrograph and rainfall field time series. The case study serving to test the proposed E-GIUH identification
 117 method is described in Section 3. This case study combines a set of events affecting two basins located in
 118 Southern France. Section 4 provides the application conditions of this E-GIUH identification approach, and
 119 Section 5 discusses the results obtained. Section 6 concludes the manuscript.

120

121 2. Methods

122 2.1 The Event-specific Geomorphological Instantaneous Unit Hydrograph (E-GIUH)

123 This section introduces the spatial variability of rainfall in the derivation of the Width Function-based E-
 124 GIUH (D’Odorico and Rigon, 2003; Rigon et al., 2016). The travel time of water drops and the GIUH both
 125 depend primarily on the hydrological distance L , defined as the distance to the outlet from any point on the
 126 hydrological network. Let w be the width function of the basin, defined as the portion of the basin area at the
 127 hydrological distance L , which in addition represents the transverse extent of the basin at L (Rodriguez-Iturbe
 128 and Rinaldo, 1997). The spatial rainfall variability is represented by the rainfall variability along hydrological
 129 paths (Smith et al., 2005). The flow at the catchment outlet can be expressed as:

$$130 \quad Q(t) = \int_0^{L_{max}} dQ(L, t) dL \quad \text{with} \quad dQ(L, t) = A w(L) dL \int_0^t R_e(L, t - \tau) f(L, \tau) d\tau \quad (1)$$

131 with: $dQ(L, t)$ denoting the outflow at time t from surface area $dA = A w(L)dL$ at hydrological distance L ; R_e
 132 the effective rainfall at time τ and at hydrological distance L ; L_{max} the maximum hydrological distance; and f
 133 the travel time distribution of water particles from dA .

134 It is assumed that the probability density function (pdf) of travel time can be modeled by the following law
 135 (Rigon et al., 2016; Rinaldo et al., 1991):

$$136 \quad f(L, t) = \frac{L}{\sqrt{4\pi D(L) t^3}} \exp \left[-\frac{(L-U(L)t)^2}{4D(L)t} \right] \quad (2)$$

137 with $U(L)$ and $D(L)$ denoting the respective parameters of velocity and coefficient of dispersion (sometimes
 138 called diffusivity) of the travel time pdf. Let's note that Eq. (2) is also the (Hayami, 1951) solution of the
 139 Diffusive Wave Equation (Moussa, 1997) with (U, D) standing for the mean velocity and coefficient of
 140 dispersion, respectively, of the wave flow. The influence of rainfall spatial variability on flow conditions may
 141 explain why U and D both depend on L .

142 The rainfall variability along flow paths can be introduced by defining the rainfall width function, as inspired
 143 from (Smith et al., 2005):

$$144 \quad w_R(L, t) = \frac{R_e(L, t)}{\overline{R_e(t)}} w(L) \quad (3)$$

145 with w_R rainfall width function, and $\overline{R_e(t)}$ mean value of effective rainfall over the basin at time τ .

146 Unlike the width function, the rainfall width function does depend on time. (Emmanuel et al., 2015) showed
 147 that the influence of spatial rainfall variability on the basin response is well explained by the deviation between
 148 the width function and the rainfall width function associated to the pattern of rain amount during a time interval
 149 of approximately two to three times the basin response time, which is thus close to the time of concentration. The
 150 event rainfall width function w_E is defined over this duration; it was first introduced by (Woods and Sivapalan,
 151 1999) to analyze the effect of spatial rainfall variability and runoff formation on catchment response. According
 152 to these authors, it can be assumed that the spatio-temporal variability of rainfall along flow paths can be written
 153 as the product of two independent functions, i.e.:

$$154 \quad R_e(L, t) = w_E(L) \overline{R_e(t)} \quad (4)$$

155 with w_E event rainfall width function which depends only on hydrologic distance and $\overline{R_e}$ hyetograph of effective
 156 rainfall which depends only on time.

157 Introducing Eq. (4) into Eq. (1) leads to the following expression of outflow:

$$158 \quad Q(t) = \int_0^{L^{max}} A w_E(L) dL \int_0^t R_e(L, t - \tau) f(L, \tau) d\tau \quad (5)$$

159 which can also be written :

$$160 \quad Q(t) = A \int_0^t \overline{R_e(t - \tau)} f_E(\tau) d\tau \quad \text{with} \quad f_E(\tau) = \int_0^{L^{max}} w_E(L) f(L, \tau) dL \quad (6)$$

161 f_E is the E-GIUH associated with the flood event E. (Saco and Kumar, 2002a) stated that the pdf of travel
 162 time f can be approximated by replacing the varying parameters U and D by an equivalent network velocity
 163 (U_E) and equivalent hydrodynamic coefficient of dispersion (D_E), which enable preserving the mean and

164 variance of f_E . They noticed that “although used as spatially invariant parameters, they are estimated to account
 165 for the nonlinear effects that arise when varying hydrodynamic parameters”.

166 Ultimately, the expression of E-GIUH is:

$$167 \quad f_E(t) = \int_0^{L_b} \frac{L w_E(L)}{\sqrt{4\pi D_E t^3}} \exp\left[-\frac{(L - U_E t)^2}{4 D_E t}\right] dt \quad (7)$$

168 In addition, (Rodriguez-Iturbe and Rinaldo, 1997) found that the first two moments of f_E must satisfy the
 169 following expressions:

$$170 \quad E(T) = \frac{1}{U_E} E(L) \text{ and } Var(T) = 2 \frac{D_E}{U_E^2} E(L) + \frac{1}{U_E^2} Var(L) \quad (8)$$

171 where $E(L)$ and $Var(L)$ are the first two moments of the pdf of hydrological paths.

172 In sum, the spatial variability of rainfall can be integrated into the width function-based GIUH by replacing
 173 the width function by the rainfall width function. This formulation paves the way to determining the E-GIUH,
 174 which characterizes the basin response to each rain event forcing.

175 2.2 Principles of the E-GIUH identification process

176 The problem posed consists of identifying the E-GIUH, specific to flood event E that leads to the best
 177 reconstitution of the observed hydrograph at the basin outlet. This E-GIUH is defined by two parameters U_E and
 178 D_E as well as by the event rainfall width function w_E . Note that Equation (6) expresses the hydrograph as a
 179 function of both E-GIUH and the hyetograph of effective rainfall, meaning that the identification of effective
 180 rainfall and Event-GIUH are not independent of one another and moreover that the transformation of observed
 181 rainfall data fields into a hyetograph of effective rainfall might influence the identified E-GIUH. For this reason,
 182 the components of the hyetograph of effective rainfall are also considered as parameters. Nevertheless, the
 183 adopted identification algorithm (Section 4) provides the opportunity to introduce the hyetograph of effective
 184 rainfall as an “*a priori*” information to which a level of confidence is ascribed, thus making it possible to control
 185 its influence on the result. Lastly, the E-GIUH identification process calls for a model capable of combining the
 186 following equations:

187 i) Flow at the catchment outlet expressed as the convolution product: $Q = \overline{R}_e * f_E(U_E, D_E)$, written in a
 188 discretized manner:

$$189 \quad Q_j = A \sum_{k=1}^{k=j} \overline{R}_{e_{j+1-k}} f_{E_k}(U_E, D_E) \quad (9)$$

190 with:

$$f_{E_k}(U_E, D_E) = \sum_{\gamma=1}^{\gamma=n_w} w_{R\gamma} \int_{(k-1)\Delta t}^{k\Delta t} \frac{\bar{L}_\gamma}{\sqrt{4\pi D_E \tau^3}} \exp\left[-\frac{(\bar{L}_\gamma - U_E \tau)^2}{4D_E \tau}\right] d\tau \quad (10)$$

where: $\mathbf{Q} = (Q_1, Q_2, \dots, Q_{m_q})$ is the vector grouping the m_q components of the event hydrograph, $\bar{\mathbf{R}}_e = (\bar{R}_{e_1}, \bar{R}_{e_2}, \dots, \bar{R}_{e_{m_r}})$ the vector grouping the m_r components of the hyetograph of effective rainfall over the basin, and $\mathbf{w}_E = (w_{E_1}, w_{E_2}, \dots, w_{E_{n_w}})$ the vector grouping the n_w components of the event rainfall width function at distances $(L_1, L_2, \dots, L_{n_w})$. The vector $\mathbf{f}_E = (f_{E_1}, f_{E_2}, \dots, f_{E_{m_r}})$ regroups the m_r components of the E-GIUH.

ii) A conservation equation stating that runoff volume at the outlet amounts to the effective rainfall:

$$\sum_{k=1}^{k=m_q} Q_k = A \sum_{k=1}^{k=m_r} \bar{R}_{e_k} \quad (11)$$

iii) The discretized form of Equations (8), which relate the parameters of the E-GIUH with the pdf of hydrological distances, in the framework of GIUH theory:

$$E(T, U_E, D_E) - \frac{\bar{L}}{U_E} = 0 \quad (12)$$

$$Var(T, U_E, D_E) - 2 \frac{D_E}{U_E^2} \bar{L} + \frac{1}{U_E^2} V(L) = 0 \quad (13)$$

with:

$$\bar{L} = \sum_{\gamma=1}^{\gamma=n_w} w_{E\gamma} L_\gamma \text{ and } V(L) = \sum_{\gamma=1}^{\gamma=n_w} w_{E\gamma} [L_\gamma - \bar{L}]^2 \quad (14)$$

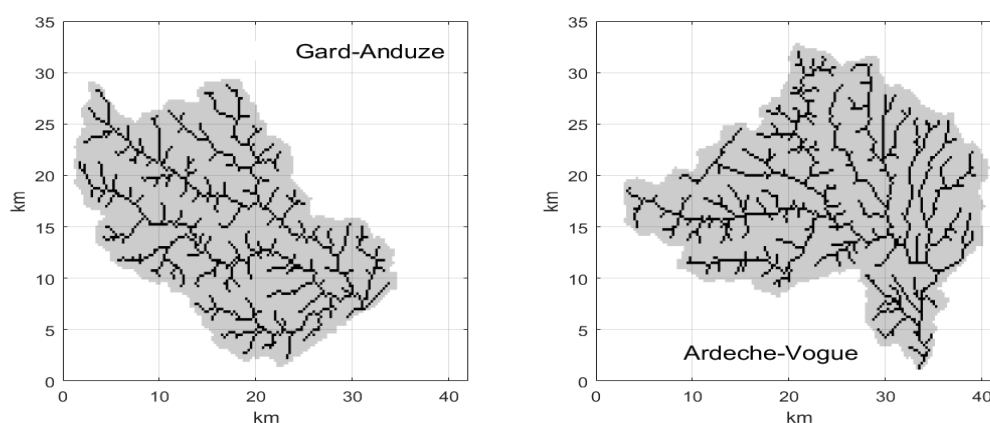
Moreover, the vector of parameters to identify is: $\mathbf{p} = (U_E, D_E, \bar{\mathbf{R}}_e)$, while the vector grouping the data associated with Equations 9, 11, 12 and 13, used to base the identification procedure is: $\mathbf{d}_0 = (\mathbf{Q}_0, \sum_{k=1}^{k=m_r} Q_{0k}, 0.0, 0.0)$.

3. Case study and dataset

The Cevennes Region encompasses a medium-elevation mountain range located in the southeastern part of France's Massif Central sector (Fig. 1). The southeastern end of this range consists of a plateau and a plain area extending to the Mediterranean Coast. Several rivers originate in the Cevennes Mountains and cross the intermediate plain to empty into the Rhone River or flow into the Mediterranean Sea. This region displays typical Mediterranean climate and is subject to heavy rainfall events during the fall, causing flash floods that can result in considerable damage and losses. The Cevennes Region is covered by a network of rain gauges at a density of roughly 1 gauge every 150 km², complemented by two weather radars that provide quantitative precipitation estimates (QPE) at a high spatial (1 km x 1 km) and temporal (5 min) resolution.

218 Hydrometeorological recordings in this region are enhanced by the presence of the OHMCV (Cevennes-Vivarais
219 Mediterranean Hydrometeorological Observatory) (<http://www.ohmcv.fr>). This long-term observatory has built
220 an integrated hydrometeorological database of flash flood events across the Cevennes-Vivarais area. The
221 available operational datasets have therefore undergone a thorough quality control and can be considered highly
222 accurate (Boudevillain et al., 2011). The OHMCV provides several QPE products. For purposes of this study,
223 the hourly rainfall fields of 1 km x 1 km spatial resolution, obtained by means of a radar - rain gauge merging
224 technique proposed by (Delrieu et al., 2014) have been used; these fields offer a high level of accuracy compared
225 to other QPE products.

226 The basins considered herein are: Gard at the Anduze gauging station (surface area: 545 km²), and Ardèche
227 at the Vogüe gauging station (620 km²). Upstream of Anduze, the Gard bedrock consists mainly of schist (61%)
228 and granite (18%). The Ardèche bedrock upstream of Vogüe is mostly granitic (72%) (Douinot et al., 2018). The
229 hydrographic network of these two basins has been determined with the TauDem tool (Tarboton, 1997), in using
230 a DTM at a spatial resolution of 250 m. Both basins are well documented and have been the subject of several
231 works on rainfall-runoff modeling (Adamovic et al., 2015; Douinot et al., 2018; Moussa et al., 2007; Naulin et
232 al., 2013; Saulnier and Le Lay, 2009; Trambly et al., 2011; Vannier et al., 2016) and flash flood forecasting
233 (Alfieri et al., 2011; Dolcine et al., 2001).



234

235

Figure 1: Case study of the two basins studied

236

237 The QPE product covers a time period from 2011 to 2014 and includes one very intense and significant rain
238 event in September 2002 (Delrieu et al., 2005). A sample of six flood events at each basin have been selected,
239 comprising both rain and flow data. All these events are single-peak hydrographs, which are more easily adapted
240 to characterizing a unit hydrograph. Some selected events occurred during long rainy periods, which explains the
241 high flow values observed upon their initiation. The main features of these flood events are summarized in Table

242 1. The peak flow of a two-year return period is, respectively, $Q_2 = 630 \text{ m}^3/\text{s}$ for Gard-Anduze and $Q_2 = 740 \text{ m}^3/\text{s}$
 243 for Ardèche-Vogüe, thus indicating that the dataset contains flow events of various magnitudes. The coefficient
 244 of variation in the spatial rainfall amount ranges from 0.08 to 1.04 for Gard-Anduze and from 0.22 to 0.76 for
 245 Ardèche-Vogüe, which confirms the varied characteristics of the selected flood events.

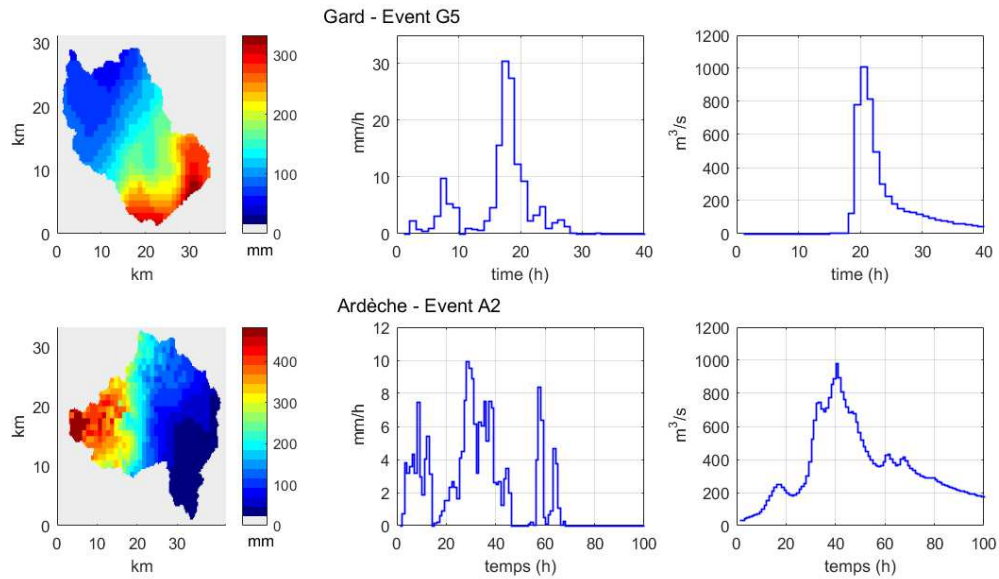
246

247

Basin	Flood Event	Peak flow (m ³ /s)	Rainfall duration (h)	Rainfall amount (mm)	Rainfall variability (coef. var)
Gard (Anduze) 545 km ²	1 Oct 8-9, 2002	2,744	23	294.6	0.44
	2 Oct 20-23, 2008	933	10	125.8	1.04
	3 Oct 31 - Nov 3, 2008	1,010	61	287.8	0.25
	4 Oct 29 - Nov 1, 2010	306	41	191.1	0.08
	5 Sept 17-21, 2014	1,010	25	148.8	0.50
	6 Nov 14, 2014	616	17	98.9	0.38
Ardèche (Vogüe) 620 km ²	1 Oct 20-23, 2008	953	26	158.6	0.31
	2 Oct 31 - Nov 3, 2008	983	44	169.3	0.76
	3 Sept 6-8, 2010	1,270	30	225.1	0.22
	4 Dec 21-24, 2010	571	56	153.6	0.22
	5 Oct 22-25, 2013	850	28	126.1	0.27
	6 Oct 9-15, 2014	1,090	48	181.4	0.66

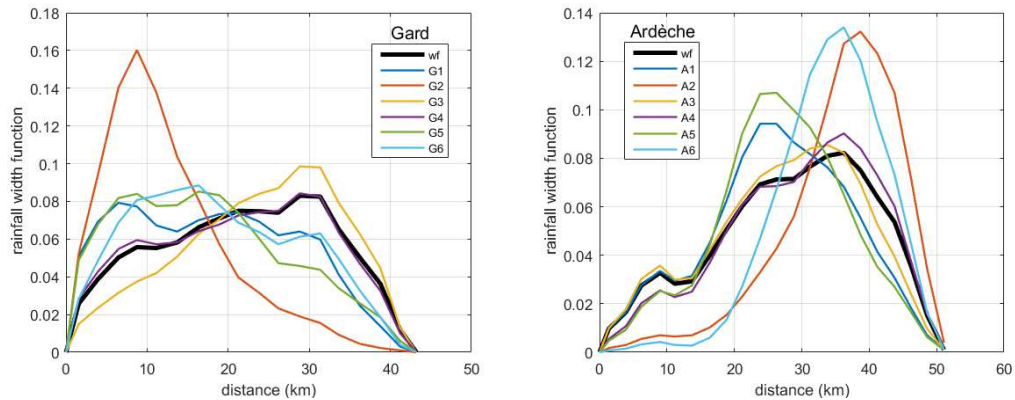
248

Table 1: Characteristics of the selected flood event



249
 250
 251
 252
 253
 254

Figure 2: Examples of flood events – Map of total rainfall (left) – Hyetograph (center) – Hydrograph (right)
 (The 12 flood events of the data set are displayed in supplementary material)



255
 256
 257
 258
 259

Figure 3: Rainfall width functions of the studied flood events - the left graph combines the six Gard-Anduze Basin events and the right graph the Ardèche-Vogüe Basin event. The thick black continuous line provides the width function of each basin.

260
 261
 262
 263
 264
 265

Figure 2 illustrates one event for each basin: G5 for Gard A2 for Ardèche. The other events of each basin are displayed in the Supplementary Information section. It can be noted that the rainfall map of Event G5 indicates that the maximum rainfall occurs downstream, as confirmed by the corresponding rainfall width function shown in Figure 3 (left graph). The rainfall map of Event A2 is quite different, with the maximum rainfall being located upstream, which has been clearly confirmed by the associated rainfall width function (Fig. 3, right graph). The rainfall width functions presented in Figure 3 reveal that most rain events feature significant variability along the

266 hydrological path, and moreover the events of the two basins are of a different nature. For Gard-Anduze (left
 267 graph), all events but one are characterized by a higher rainfall amount downstream, while for Ardèche-Vogüe
 268 most rain events are characterized by a higher rainfall amount upstream or in the central part of the basin. It is
 269 clear that these rainfall features can influence the basin response to rainfall forcing, along with the E-GIUH
 270 summarizing this response.

271

272 4. Application and results

273 4.1 The identification algorithm

274 It has been proposed to treat E-GIUH identification within the framework of inverse theory, as detailed in the
 275 textbooks by (Menke, W. 2012; Tarentola, A., 2005).

276 The solution minimizes the following expression:

$$277 \Phi(\mathbf{d}, \mathbf{p}) = [\mathbf{m}(\mathbf{d}) - \mathbf{d}]^t \mathbf{C}_Q^{-1} [\mathbf{m}(\mathbf{p}) - \mathbf{d}_0] + [\mathbf{p} - \mathbf{p}_0]^t \mathbf{C}_P^{-1} [\mathbf{p} - \mathbf{p}_0] \quad (15)$$

$$278 \mathbf{d} = m(\mathbf{p})$$

279 where: Φ is the likelihood function, t signifies transpose, m denotes the model relating data and parameters, \mathbf{p}_0 is
 280 the vector of *a priori* parameters, \mathbf{C}_p is the covariance matrices of residuals between truth (and unknown) and *a*
 281 *priori* parameters, and \mathbf{C}_{dm} the covariance matrix combining data and modeling uncertainties (Tarentola, A.,
 282 2005).

283 The statistical distributions of both $[\mathbf{d} - \mathbf{d}_0]$ and $[\mathbf{p} - \mathbf{p}_0]$ are assumed to be unbiased and Gaussian. Menke
 284 (1989) demonstrated that the solution vector \mathbf{p}' satisfies:

$$285 \mathbf{p}' = \mathbf{p}_0 + \mathbf{C}_p \mathbf{M}^t [\mathbf{M}^t \mathbf{C}_p \mathbf{M} + \mathbf{C}_{dm}]^{-1} [\mathbf{d}_0 - m(\mathbf{p}') + \mathbf{M}(\mathbf{p}' - \mathbf{p}_0)] \quad (16)$$

286 where \mathbf{M} is the matrix of (first-order) partial derivatives of model m . If model m is nonlinear, (Tarentola, A.,
 287 2005) demonstrated that the solution can be obtained using a quasi-Newton method by means of the following
 288 algorithm (Equation 3.51, p. 69):

$$289 \mathbf{p}_{n+1} \approx \mathbf{p}_n - \mu_n [\mathbf{M}_n^t \mathbf{C}_p^{-1} \mathbf{M}_n + \mathbf{C}_d^{-1}]^{-1} [\mathbf{M}_n^t \mathbf{C}_{dm}^{-1} \langle m(\mathbf{p}_n) - \mathbf{d}_0 \rangle + \mathbf{C}_p^{-1} \langle \mathbf{p}_n - \mathbf{p}_0 \rangle] \quad (17)$$

290 in which \mathbf{P}_n constitutes the result of the n^{th} iteration, $\mathbf{M}_n = \frac{\partial \mathbf{m}(\mathbf{p}_n)}{\partial (\mathbf{p}_n)}$ is the matrix of (first-order) partial
 291 derivatives of the model at point \mathbf{p}_n , and $\mu_n < 1$ serves to control the convergence. More information regarding
 292 the resolution of such nonlinear problems can be found in (Menke, 2012; Tarentola, A., 2005).

293 The *a priori* information, introduced in terms of $(\mathbf{p}_0, \mathbf{C}_p)$, contains the initial knowledge of the parameters to
 294 be identified, along with the confidence ascribed to this knowledge. If the observed data are insufficient or if the
 295 level of confidence in the data is low, then the problem becomes underdetermined and the *a priori* information
 296 assumes a dominant role. If the problem is over-determined (i.e. availability of very high quality data in
 297 sufficient quantity), the solution would only depend very little on the *a priori* information.

298 The next section presents the application conditions of this inverse algorithm in order to identify the E-GIUH
 299 by focusing on the *a priori* information that initializes the identification process.

300 4.2 Identification algorithm – A priori information

301 4.2.1 Data and associated covariance matrix

302 The data vector, which regroups $n_d = m_q + 3$ components, $\mathbf{d}_0 = (\mathbf{Q}_0, \sum_{k=1}^{k=m_r} Q_{0k}, 0.0, 0.0)$, was introduced
 303 in Section 2.2. Its covariance matrix \mathbf{C}_{dm} characterizes the uncertainties on both the data and model equations.
 304 This matrix is assumed to be diagonal, and the standard deviations associated with both the data and model
 305 equations have been assembled in the vector $\boldsymbol{\sigma}_{\mathbf{d}_0} = (\boldsymbol{\sigma}_{\mathbf{Q}_0}, \sigma_{\Sigma Q_0}, \sigma_E, \sigma_V)$, with:

$$306 \quad \boldsymbol{\sigma}_{\mathbf{Q}_0} = (\sigma_{Q_1}, \dots, \dots, \sigma_{Q_{m_q}}) \text{ and } \sigma_{Q_{0i}} = \max[\alpha_Q Q_{0i}, \sigma_{Q_{min}}] \quad (17)$$

$$307 \quad \sigma_{\Sigma Q_0} = \alpha_{\Sigma} \left[\sum_{k=1}^{k=m_q} Q_k \right]$$

$$308 \quad \sigma_E = \alpha_E E(T, U_e, D_e)$$

$$309 \quad \sigma_V = \alpha_V \text{Var}(T, U_e, D_e)$$

310 $\alpha_{\Sigma}, \alpha_E, \alpha_V$ are the coefficients of variation of the errors associated with Equations (11), (12) and (13),
 311 respectively.

312 4.2.2 A priori E-GIUH parameters

313 The two E-GIUH parameters are velocity (U_E) and the coefficient of dispersion (D_E). Nevertheless, the E-
 314 GIUH components also depend on the event rainfall width function (\mathbf{w}_E), which reveals the spatial pattern of

315 effective rainfall. The rainfall width function is derived from radar time series data; let's note that this choice is
 316 associated with the measured rainfall width function and not the effective rainfall width function. Such caution is
 317 exercised in seeking to maintain the E-GIUH independent of the *a priori* effective rainfall, which may be
 318 erroneous. Comparison tests conducted between rainfall width functions and effective rainfall width functions,
 319 by means of the Kolmogorof-Smirnov protocol, have confirmed that the two pdfs are not significantly different.

320 The *a priori* velocity (U_{E0}) and *a priori* hydrodynamic coefficient of dispersion (D_{E0}) are both set by the
 321 user and accompanied by their standard deviations of σ_U and σ_D , respectively.

322 The total coefficient of dispersion of the GIUH is expressed as follows (Rodriguez-Iturbe and Rinaldo,
 323 1997):

$$324 \quad D_{G0} + D_{E0} = \frac{U_{E0}^2 \text{Var}(T)}{2L} \text{ and } D_{G0} = \frac{U_{E0} \text{Var}(L)}{2L} \quad (18)$$

325 4.2.3 *A priori* parameters: Hyetograph of effective rainfall \mathbf{R}_e

326 The GIUH expresses the transformation of effective rainfall over the basin to flow at its outlet. It is worth
 327 considering the accuracy of effective rainfall. The hydrograph of effective rainfall is incorporated into the
 328 parameters of the inverse algorithm and moreover defined by its *a priori* components (\mathbf{R}_{n0}) as well as the
 329 associated error covariance matrix. The inverse algorithm offers a flexibility that enables taking the effective
 330 rainfall into account in various ways, ranging between two extreme situations, namely:

331 i) the basin production function, giving rise to a vector grouping the *a priori* hyetograph of effective rainfall
 332 components (\mathbf{R}_{e0}), is considered to be accurate, and the associated covariance terms are very weak. The inverse
 333 algorithm does not significantly modify the *a priori* hyetograph of effective rainfall, and its functioning is nearly
 334 the equivalent to the calibration of the two parameters defining the E-GIUH;

335 ii) the production function is unknown, and the hyetograph of effective rainfall components are the
 336 parameters to be determined. In this case, (\mathbf{R}_{e0}) is not considered to be accurate, and the associated covariance
 337 terms are assigned large values. The inverse algorithm identifies both the net hyetograph and E-GIUH and
 338 moreover may be viewed as an evolution of the method developed by (Duband et al., 1993) to simultaneously
 339 identify the unit hydrograph common to all events and the hyetograph of effective rainfall of each of them.

340 The matrix of error covariance of the effective rainfall hyetograph is defined as follows:

$$341 \quad \text{cov}(R_{e0i}, R_{e0j}) = \sigma_{Ri} \sigma_{Rj} \exp \left[- \left(\frac{|i-j|\Delta t}{T_R} \right)^2 \right] \text{ with } \sigma_{Ri} = \max(\alpha_R R_{e0i}, \sigma_{Rmin}) \quad (19)$$

342 with i and j being time indices, σ_{R_i} and σ_{R_j} the error standard deviation of R_{e0i} and R_{e0j} , respectively. α_R is the
343 coefficient of variation in the error characterizing the hyetograph of effective rainfall, β_R denotes the minimum
344 value assigned to the error standard deviation, and T_R is the decorrelation time controlling the temporal structure
345 of the errors affecting successive components of the *a priori* net hyetograph.

346 The role of the *a priori* net hyetograph in the E-GIUH identification is defined by the value assigned to α_R . A
347 very weak value, e.g. 0.05, means that the *a priori* net hyetograph is assumed to be highly accurate, whereas a
348 larger value, e.g. 0.2 to 0.3, indicates that the *a priori* net hyetograph is assumed to be inaccurate.

349 4.3 Reference E-GIUHs

350 4.3.1 Data and model description

351 The flow data are assumed to be of good quality. The coefficient of variation of the flow measurement error
352 has been set at $\alpha_Q = 0.10$, with a minimum value of $2m^3s^{-1}$. Equation (9) is assumed to be exact and free of
353 any error. Equation (11), which expresses the budget equation and is assumed to be associated with a weak error
354 characterized by its small coefficient of variation, $\alpha_\Sigma = 0.05$. The theoretical GIUH framework coupled with the
355 introduction of the spatial rainfall variability accurately depicts the true E-GIUH (Equations 12 and 13). This
356 modeling error is then defined by weak coefficients of variations: $\alpha_E = 0.05$ and $\alpha_V = 0.05$, respectively.

357

358 4.3.2 *A priori* E-GIUH

359 A constant *a priori* velocity has been adopted for all flow events of the same basin. The standard deviation
360 values retained are $\sigma_U = 0.5ms^{-1}$ and $\sigma_D = 1000 m^2s^{-1}$, in order to leave a wide interval of variation with
361 respect to the *a priori* values. The *a priori* E-GIUH also depends on the rainfall width function w_{E0} , which has
362 been derived from radar time series data. Let's note once again that this choice is associated with the measured
363 rainfall width function and not the effective rainfall width function. Such an exercise of caution aims to maintain
364 the E-GIUH independent of the *a priori* effective rainfall, which may be erroneous. In addition, the comparison
365 of rainfall width functions and effective rainfall width functions for these case study events, by means of the
366 Kolmogorof-Smirnov test, have confirmed that they do not differ significantly.

367 The SCS model has been adopted to provide the *a priori* values of the net hyetograph. This classical model is
368 widely used, and recent tools have been developed to derive the curve number values from remote sensing data

369 (Ross et al., 2018; Zeng et al., 2017). The SCS model has been successfully applied to basins subject to flooding
 370 in this Mediterranean region (Naulin et al., 2013). It is being used herein by considering a parameter, S_{moy} , that
 371 represents the mean storage capacity of the basin for a given event. The runoff volume is defined by:

$$372 \quad Vr = \sum_{k=1,p} \frac{(Rt_k - Ia_k)^2}{(Rt_k - Ia_k) + S_k} \quad (20)$$

373 with Vr denoting the runoff volume at the basin outlet, p the number of meshes in the basin grid, Rt_k the rainfall
 374 amount, S_k the storage capacity, and $Ia_k = 0.2 S_k$ the initial loss of mesh k . The CN values are then transformed
 375 into a map of relative storage capacity, from which the storage capacity of each mesh is derived: $S_k = S_{moy} \gamma_k$,
 376 with γ_k being the relative storage capacity of mesh k . S_{moy} has been calibrated for each flood event so that the
 377 effective rainfall volume is equal to the runoff volume. As runoff generated by the effective rainfall is assumed
 378 to be the dominant process of flow generation, the base flow is removed from the observed flow values. The pre-
 379 event base flow is the measured flow at the beginning of the rain event. At the end of the event, it is assumed that
 380 the runoff contribution becomes negligible after the rain has stopped for a period equal to the basin time of
 381 concentration. The post-event base flow is the flow measured at this time. It is assumed that the base flow varies
 382 linearly between these values during the flood event. The time of concentration is estimated to be 18h for the
 383 Gard-Anduze basin and 24 h for the Ardèche-Vogüe basin. Changing the concentration times by a few hours
 384 don't significantly affect the obtained results. The net hyetograph (R_{e0}) is thus deduced from the time series of
 385 hourly effective rainfall maps.

386 For the identification of the reference E-GIUH, it is assumed that the *a priori* effective rainfall is highly
 387 accurate. The coefficient of variation of each net hyetograph component is then given by the value $\alpha_R = 0.10$. In
 388 addition, $T_R = 2 h$ controls the temporal structure of the error on the *a priori* net hyetograph.

389 The application conditions selected to derive the reference E-GIUHs are collated in Table 2

Hydrological distance increment: $\Delta L = 2500 \text{ m}$

Data and model errors:

Error on flow: $\alpha_Q = 0.10$

Conservation of flux – Eq. (17): $\alpha_\Sigma = 0.05$

E-GIUH equation – Eq. (17): $\alpha_E = 0.05$

E-GIUH equation – Eq. (17): $\alpha_V = 0.05$

A priori parameter values:

Velocity: $U_{E0} = 1.2 \text{ ms}^{-1}$ (Gard-Anduze), $U_{E0} = 1.0 \text{ ms}^{-1}$ (Ardèche-Vogüe), $\sigma_U = 0.5 \text{ ms}^{-1}$

Coef. of dispersion provided by Eq. (18) $D_{E0} \approx D_{G0}/2$ and $\sigma_D = 1200 \text{ m}^2 \text{ s}^{-1}$

A priori net hyetograph: SCS - $\alpha_R = 0.10$ and $T_R = 2 \text{ h}$

390 Table 2: Summary of the reference applications conditions

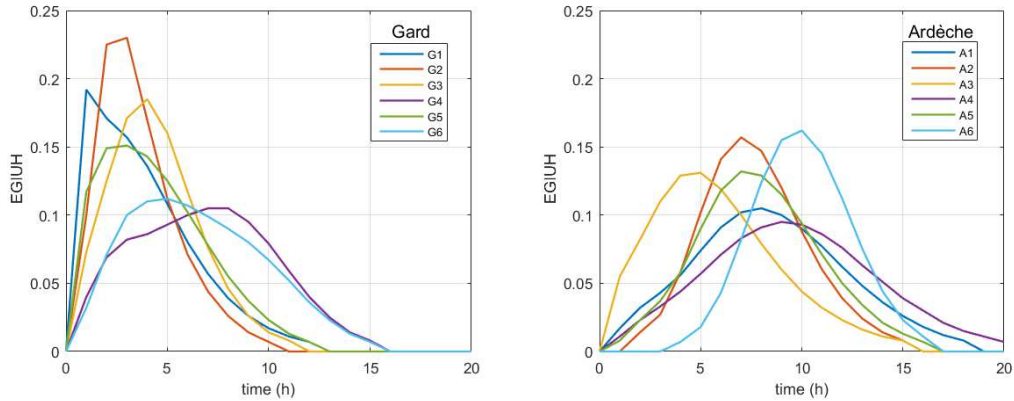
391 *4.4 Results and discussion*

392 The accuracy of the identified E-GIUH can only be evaluated indirectly. The classical Nash-Sutcliffe
393 efficiency criterion (denoted NSE) is used for such a purpose:

394
$$NSE_x = 1 - \frac{\sum_{i=1}^{i=n} (x_{ref\ i} - x_{tes\ i})^2}{\sum_{i=1}^{i=n} (x_{ref\ i} - \bar{x})^2} \quad (21)$$

395 with $[x_{ref\ i}]$ reference vector of n components of mean \bar{x}_{tes} , $[x_i]$ vector to be tested.

396 The E-GIUHs identified according to the reference application conditions are displayed in Figure 4.



397
398 Figure 4: Identified Event-GIUHs relative to the reference application conditions

399
400 These results have been assessed by calculating four criteria: 1) NSE_Q between observed hydrographs and
401 hydrographs modeled using *a priori* E-GIUH and an *a priori* net hyetograph; 2) NSE_Q between observed
402 hydrographs and hydrographs modeled using the identification results; 3) NSE_{Rn} between the *a priori* net
403 hyetograph and the identified net hyetograph; and 4) NSE_{GIUH} between the *a priori* E-GIUH and the identified

404 E-GIUH. These criteria are calculated for each flood event; their average value is computed for the two basins so
 405 as to provide an overview of the results obtained. These criteria have been compiled in Table 3, leading to the
 406 following comments:

407 - The identified E-GIUHs allow improving the simulation of observed hydrographs. This improvement seems
 408 as more pronounced as the identified values of (U_E, D_E) differ from the *a priori* values. The average increase in
 409 NSE_Q is significant, from 0.72 to 0.83 for Gard-Anduze and from 0.65 to 0.84 for Ardèche-Vogüe.

410 - This increase primarily results from an evolution in E-GIUHs. Indeed, a comparison of the net hyetographs
 411 indicates that the *a priori* ones slightly differ from the identified ones. The average value of NSE_{Rn} equals 0.97
 412 for Gard-Anduze and 0.96 for Ardèche-Vogüe; in all cases, the criterion is above 0.92.

413 - A comparison of the *a priori* and identified E-GIUHs confirms quite well that based on the reference
 414 conditions, the identification method acts primarily on E-GIUHs. Indeed, the average values of NSE_{GIUH} , 0.74
 415 for Gard-Anduze and 0.65 for Ardèche-Vogüe, underscore that *a priori* E-GIUHs differ considerably from
 416 identified ones.

417 Beyond these criteria, it is very interesting to note the wide diversity and wide variability of the E-GIUHs of
 418 each basin. For instance, the time to peak for Gard-Anduze flood events (left graph) ranges from one hour to
 419 seven hours, while the time to peak for Ardèche-Vogüe flood events ranges from 5 to 10 hours. These results
 420 confirm not only the influence of rainfall variability on the E-GIUH, but also the fact that the E-GIUH could be
 421 well adapted to serve as a signature characteristic of a flood event.

422
 423
 424
 425
 426
 427
 428
 429

Basin	Flood event	<i>A priori</i> parameters		Identified parameters		Evaluation criteria			
		U_{E0} (m/s)	D_{E0} (m ² /s)	U_E (m/s)	D_E (m ² /s)	1 NSE_Q A <i>priori</i>	2 NSE_Q Identified	3 NSE_{Rn}	4 NSE_{GIUH}
Gardo (Anduze) 545 km ²	G1	1.2	1,700	1.54	5,180	0.77	0.83	0.92	0.72
	G2	1.2	1,219	1.24	958	0.86	0.88	0.99	0.99
	G3	1.2	1,129	1.78	4,209	0.73	0.92	0.99	0.06

	G4	1.2	1,476	1.03	873	0.51	0.75	0.97	0.87
	G5	1.2	1,693	1.47	2,323	0.69	0.75	0.97	0.90
	G6	1.2	1,464	0.93	1,000	0.76	0.92	0.96	0.83
	Average	1.2	1,447	1.33	2,425	0.72	0.84	0.97	0.73
Ardèche (Vogüe) 620 km ²	A1	1.0	970	1.00	1,548	0.80	0.89	0.96	0.98
	A2	1.0	493	1.45	2,605	0.71	0.94	0.97	-0.31
	A3	1.0	1,059	1.36	4,330	0.50	0.79	0.93	0.33
	A4	1.0	937	0.96	1,540	0.80	0.87	0.99	0.97
	A5	1.0	768	1.13	1,460	0.64	0.85	0.93	0.87
	A6	1.0	383	1.09	652	0.46	0.77	0.92	0.90
	Average	1.0	768	1.17	2,022	0.65	0.85	0.95	0.63

430

431 Table 3: Results for the 12 studied events – Comparison of *a priori* and final parameters and evaluation

432 criteria

433

434 The *a priori* values of the E-GIUH parameters (U_{E0} , D_{E0}) have been chosen regardless of the event features.

435 What conclusions can be drawn from their resulting values? For the sake of simplicity, the hydrological features

436 of a flood event are summarized by its specific flow peak (q_{max}), considered as an indicator of the event

437 magnitude. The use of a specific flow peak allows regrouping the events of both catchments on the same graph

438 in order to study a possible relationship between this indicator and the E-GIUH parameters. The scattergrams

439 (U_E , q_{max}) and (D_E , q_{max}) with q_{max} as the specific flow peak are displayed in Figure 5. It can be observed that

440 a significant correlation exists between the two E-GIUH parameters and the specific flow peak. Let's note that

441 the coefficient of determination (R^2) has been calculated without accounting for the exceptional flow event that

442 occurred on Sept 20-21, 2002. The limited size of the dataset and the fairly low value of R^2 do not offer the basis

443 for a more detailed analysis. This result however could suggest that:

444 - The mean flow velocity U_E increases with the magnitude of the flood event, which appears to be logical and

445 consistent with previous results. It is interesting to note that taking the rainfall width function into consideration

446 does not alter this mean trend, even though it could be surmised that flood events displaying a strong rainfall

447 variability also exhibit a stronger variability in flow velocity within the hydrological network.

448 - Results regarding the coefficient of dispersion D_E are not simple to analyze. The model equations relate D_E

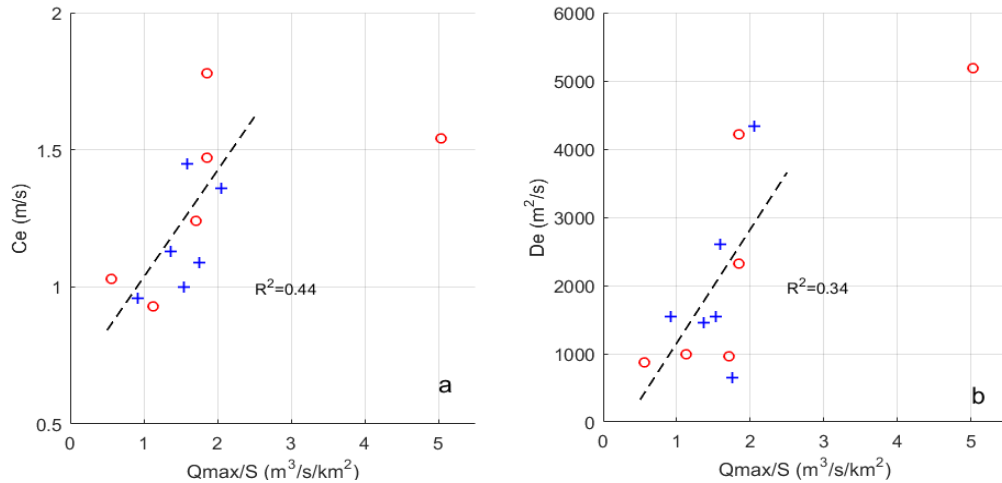
449 and U_E , which would contribute to the link between q_{max} and D_E . Similarly, the average values of D_E and U_E

450 (Table 2) indicate a strong increase in D_E values with respect to the *a priori* values, thereby likely to generate an

451 accurate restitution of the observed hydrographs. Lastly, the sensitivity study (next section) suggests that this

452 identification procedure is not highly sensitive to D_E . Moreover, it is not yet possible to draw a clear conclusion,

453 and studying a larger sample of events would allow progressing in this effort.



454

455 Figure 5: Relationship between the specific peak flow and the E-GIUH parameters of the flood events

456 *4.5 Sensitivity study of the E-GIUH identification*

457 This sensitivity study addresses the influence of the application conditions on the identified E-GIUHs. This
 458 section provides the main results and conclusions of the sensitivity study; a detailed presentation can be found in
 459 the Supporting Information. Note that special attention has been paid to the influence of the *a priori* hyetograph
 460 of effective rainfall.

461 *4.5.1 Sensitivity to (U_E, D_E) variations*

462 This test examines the influence of (U_E, D_E) variations on the simulated E-GIUHs and hydrographs. The E-
 463 GIUHs and hydrographs obtained by varying (U_E, D_E) values with respect to the reference solution are
 464 compared to the E-GIUHs and hydrographs of this reference solution by calculating the NSE values. Figure 5
 465 illustrates the results of this test, which yields two key indications: i) the influence of D_E is much weaker than
 466 that of U_E ; and ii) the simulated hydrographs are much less influenced by (U_E, D_E) variations than the simulated
 467 E-GIUHs. This latter result proves to be important, given that the identification procedure is mostly based on
 468 observed hydrographs. This sensitivity study confirms that a reliable estimation of (U_E, D_E) from hydrographs is
 469 far from being straightforward.

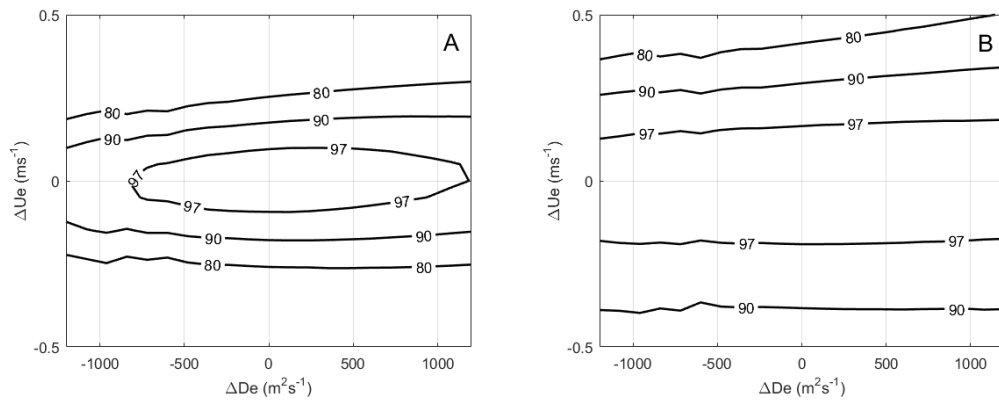


Figure 6: Sensitivity of E-GIUHs (A) and simulated hydrographs (B) to variations in (U_E, D_E)

4.5.2 Sensitivity of the E-GIUH to inverse algorithm application conditions

This part of the sensitivity study comprises: i) the confidence assigned to flow data (coefficient of variation α_Q), ii) the confidence assigned to the GIUH theoretical model (coefficients of variation α_E and α_V), iii) the influence of the *a priori* value of D_{E0} , iv) the influence of the *a priori* value of U_{E0} , and lastly v) the confidence assigned to the *a priori* hyetograph of effective rainfall (coefficient of variation α_R). It is performed by running the E-GIUH identification in varying one of these factors with respect to the reference conditions. The results obtained are summarized in Table 4 and then detailed in the Appendix.

It is interesting to emphasize the influence of an increase of α_R which controls the error variance on the *a priori* hyetograph of effective rainfall. It is confirmed that an increase of α_R results in an improvement of the restitution of the observed hydrograph. The overall improvement is obtained by changes in the resulting effective rainfall hyetograph, thus confirming the capability of this method to identify both the E-GIUH and the hyetograph of effective rainfall (Rn). This result might extend the application domain of the proposed method, but this subject is out the scope of the present work which focuses on the identification of E-GIUHs.

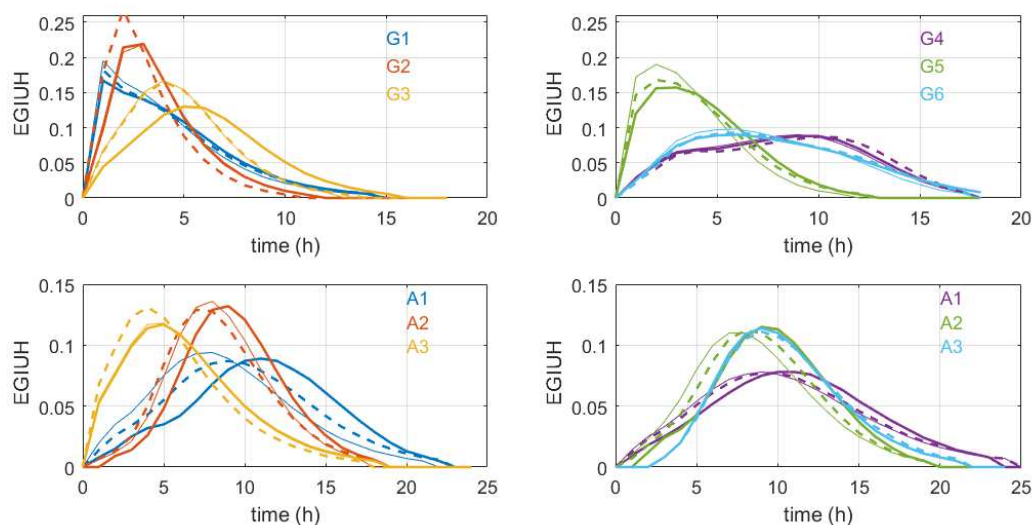
Variable	Sensitivity of the identification result	Comment
α_Q	Strong	Decrease in NSE_Q as α_Q increases.
α_E, α_V	Weak	Significant increase in the mean value of D_E as both α_E and α_V increase.
D_{E0}	Weak	Increase in the mean value of D_E as D_{E0} increases. This result is consistent with the previous section.
U_{E0}	Moderate	An <i>a priori</i> underestimation seems to be more detrimental than an overestimation. A conservative <i>a priori</i> value seems to be preferable.
α_R	Moderate to strong	The increase in α_R results in an increase of NSE_Q . The identified E-GIUHs are only slightly affected. The overall improvement is obtained by changes in the resulting effective rainfall hyetograph.

490 Table 4: Conclusions drawn from the sensitivity study

491 *4.5.3 Influence of the a priori hyetograph of effective rainfall*

492 The previous results have been obtained by considering that the widely used SCS production function
493 accurately represents basin operations. The question raised then is whether the choice of an *a priori* hyetograph
494 of effective rainfall affects the identified E-GIUHs. This test is conducted by running the method with an *a priori*
495 hyetograph of effective rainfall that's very different from the SCS one, so as to introduce a sharp contrast with
496 the reference application conditions. The selected production function (denoted CR-PI) assumes initial losses of
497 20 mm in each mesh of the basin, along with a constant runoff coefficient. For each flood event, this coefficient
498 is estimated such that the effective rainfall volume is equal to the runoff volume. The choice of the *a priori* net
499 hyetograph is the only modification adopted with respect to the reference application conditions. The two *a*
500 *priori* net hyetographs are assumed to be rather inaccurate, with an error covariance $\alpha_R = 0.25$. It then becomes
501 possible to compare the E-GIUHs identified based on the SCS and CR-PI production function, respectively. The
502 *a priori* E-GIUHs turn out to be similar for both cases. The comparison results are detailed in the Supporting
503 Information section and illustrated in Figure 6, which displays the 12 E-GIUHs obtained from the SCS
504 (continuous line) and the CR-PI (dashed line) net hyetographs, respectively. The reference E-GIUH (thin
505 continuous line) has been added to this comparison. The sensitivity test shows that for 9 of the 12 flood events,
506 the identified E-GIUH is very weakly affected by the change in *a priori* net hyetograph ($NSE_{GIUH} > 0.94$), only
507 moderately affected for 2 of them ($NSE_{GIUH} = 0.88$) and significantly affected for 1 other event (A1-
508 $NSE_{GIUH} = 0.80$). More specifically, Figure 7 indicates that the differences between the 12 E-GIUHs remain
509 quite pronounced and much larger than the fluctuations of each E-GIUH. In addition, it is confirmed that the

510 identification method serves to improve the net hyetograph, with the identified ones lying much closer than the *a*
511 *priori* ones.



512
513 Figure 7: Sensitivity of the E-GIUHs to the production function (SCS and Cr-PI). For each of the 12 flow
514 events, three E-GIUH of the same color are displayed: E-GIUH obtained with the SCS ($\alpha R = 0.25$; plain line);
515 E-GIUH obtained with CR-PI ($\alpha R = 0.25$; dashed line); reference (thin line). The two upper graphs are for
516 Gard-Anduze and the lower for Ardèche-Vogüe

517

518 5. Summary and conclusion

519 The GIUH has become a classical representation of the rapid response of a basin when adapted to rainfall-
520 runoff modeling. If the GIUH depends on the morphological features of a basin, then it is also influenced by the
521 characteristics of rainfall patterns as well as by the variability of flow path velocities. We have therefore
522 considered that an Event-specific GIUH (or E-GIUH) exists that actually characterizes the catchment response
523 under the specific conditions of each flood event. The method proposed herein to identify this E-GIUH relies on
524 the width function-based GIUH (Rigon et al., 2016), as adapted to take into account the spatial variability of
525 rainfall through replacing the width function by the rainfall width function (Emmanuel et al., 2015; Woods and
526 Sivapalan, 1999). The E-GIUH is identified from data combining time series of rain fields and observed
527 hydrographs. This E-GIUH identification has been tested on a dataset composed of 12 flood events that occurred
528 on catchments within the OHMCV Observatory territory. Despite being of limited range, this evaluation has
529 provided interesting insights, namely:

530 - The concept of E-GIUH appears to be relevant, and moreover the proposed identification method seems
531 easily applicable and flexible for users, who are now able to define the adapted application conditions;

532 - The E-GIUHs associated with the various flood events of a catchment display very distinct characteristics,
533 thus confirming that E-GIUH shape depends on the GIUH model parameters, as well as on the rainfall width
534 function, both of which are specific to the flood events;

535 - For both basins, the two E-GIUH parameters (U_E , D_E) lie within the range [0.9 m/s, 1.8 m/s] for U_E and
536 [600 m²/s, 5,200 m²/s] for D_E . These two parameters appear to be correlated with the event peak flow, which
537 serves as an indicator of flow magnitude, even though this tenuous link needs to be confirmed and warrants
538 further investigation. The identification procedure is more sensitive to parameter U_E than to parameter D_E ,
539 mainly because the direct model is not highly sensitive to this latter parameter.

540 - The results obtained appear to be fairly robust and in most cases remain relatively independent of the *a*
541 *priori* rainfall hyetograph. This result indicates that representative E-GIUHs could be derived by defining the *a*
542 *priori* effective rainfall from a widely used production function and then calibrating the two E-GIUH parameters.

543

544 This work would need to be pursued in several directions, in order to improve our knowledge and develop
545 applications relying on the E-GIUH concept, including:

546 - A more robust assessment of the proposed method seems to be a priority. This could be achieved by
547 application to a large numbers of catchments located in various climatic zones;

548 - The E-GIUH, which is mostly based on observed data, could be considered as a signature characterizing
549 flood events;

550 - The flood events that affect a basin stem from diverse conditions: moisture status of the basin, spatial and
551 temporal characteristics of the rain event. The E-GIUH associated with a given basin summarizes the basin
552 response under such conditions. An analysis of the population of E-GIUHs would pave the way to a hydro-
553 climatological catchment response to rainfall forcing;

554 - The relatively small number of basins and flood events described here does not allow a complete
555 assessment of the limitations of the method under all circumstances. For instance, the method might be less
556 suitable if the rainfall influence results from moving rainfall fields interacting with the basin (Volpi et al., 2013).
557 In addition, the method might be less efficient when the statistical framework is outside of its application
558 domain, e.g. when the distribution of error is not Gaussian or at least unimodal, or when the *a priori* conditions
559 are not relevant.

560 - The E-GIUH represents a signature of the basin response that could prove useful for various applications.
 561 First, it can be used to diagnose basin responses to rainfall forcing. The E-GIUH summarizes the basin response
 562 that stems from diverse physiographic, climatological, and meteorological conditions, such as moisture status of
 563 the basin and the spatial and temporal distribution of rainfall forcing. The E-GIUH signature can be used to
 564 compare and classify basin responses for different forcing rain events, or to analyse the influence of land use and
 565 change (e.g. recovery after wildfire) among other factors. Analysing populations of E-GIUHs that represent
 566 various conditions opens the way to hydro-climatological studies of catchment responses. Finally, it could
 567 contribute to improving lumped rainfall-runoff modelling through transfer function adapted to rainfall patterns.

568 **Nomenclature**

569	A	Surface area
570	D	Coefficient of dispersion -
571	E	Flood Event
572	$f(L, t)$	Probability density function of travel time to the catchment outlet
573	f_E	Event specific – GIUH
574	GIUH	Geomorphological Instantaneous Unit Hydrograph
575	E-GIUH	Event specific GIUH
576	L	Distance to catchment outlet along hydrological paths
577	L_{max}	Maximum hydrological distance of the basin
578	NSE	Nash-Sutcliffe efficiency criterion
579	pdf	Probability Density Function
580	$Q(t)$	Hydrograph at the outlet
581	$R(t)$	Hyetograph
582	$R_n(t)$	Effective rainfall, part of rainfall contributing to runoff
583	$\overline{R_e}(t)$	Areal Mean value of the effective rainfall
584	t	Time
585	U	Velocity
586	w	Width function at a distance
587	w_E	Event rainfall width function

588 **Acknowledgments**

589 The authors would like to express their gratitude to O.Payraastre for providing the maps of CN values for the
 590 Cevennes Region. Pierre Kirstetter acknowledges support through the NASA Ground Validation Program award
 591 NNX16AL23G.

592 **References**

- 593 Adamovic, M., Braud, I., Branger, F., Kirchner, J.W., 2015. Assessing the simple dynamical systems approach
594 in a Mediterranean context: Application to the Ardèche catchment (France). *Hydrology and Earth*
595 *System Sciences* 19, 2427–2449. <https://doi.org/10.5194/hess-19-2427-2015>
- 596 Alfieri, L., Smith, P.J., Thielen-Del Pozo, P.J., Beven, K.J., 2011. A staggered approach to flash flood
597 forecasting - Case study in the Cévennes region. *Advances in Geosciences* 29, 13–20.
598 <https://doi.org/10.5194/adgeo-29-13-2011>
- 599 Boudevillain, B., Delrieu, G., Galabertier, B., Bonnifait, L., Bouilloud, L., Kirstetter, P.E., Mosini, M.L., 2011.
600 The Cévennes-Vivarais Mediterranean Hydrometeorological Observatory database. *Water Resources*
601 *Research* 47, 1–6. <https://doi.org/10.1029/2010WR010353>
- 602 Boudhraâ, H., Cudennec, C., Andrieu, H., Slimani, M., 2018. Net rainfall estimation by the inversion of a
603 geomorphology-based transfer function and discharge deconvolution. *Hydrological Sciences Journal*.
604 <https://doi.org/10.1080/02626667.2018.1425801>
- 605 Chen, Y., Shi, P., Ji, X., Qu, S., Zhao, L., Dong, F., 2019. New method to calculate the dynamic factor–flow
606 velocity in Geomorphologic instantaneous unit hydrograph. *Scientific Reports* 9, 1–13.
607 <https://doi.org/10.1038/s41598-019-50723-x>
- 608 Choi, Y.-J., Lee, G., Kim, J.-C., 2011. Estimation of the Nash Model Parameters Based on the Concept of
609 Geomorphologic Dispersion. *Journal of Hydrologic Engineering* 16, 806–817.
610 [https://doi.org/10.1061/\(ASCE\)HE.1943-5584.0000371](https://doi.org/10.1061/(ASCE)HE.1943-5584.0000371)
- 611 Delrieu, G., Ducrocq, V., Gaume, E., Nicol, J., Payrastré, O., Yates, E., Kirstetter, P.-E., Andrieu, H., Ayrat, P.-
612 A., Bouvier, C., Creutin, J.-D., Livet, M., Anquetin, S., Lang, M., Neppel, L., Obled, C., Parent-Du-
613 Châtelet, J., Saulnier, G.-M., Walpersdorf, A., Wobrock, W., 2005. The catastrophic flash-flood event
614 of 8-9 September 2002 in the Gard Region, France: A first case study for the Cévennes-Vivarais
615 Mediterranean Hydrometeorological Observatory. *Journal of Hydrometeorology* 6.
616 <https://doi.org/10.1175/JHM-400.1>
- 617 Delrieu, G., Wijbrans, A., Boudevillain, B., Faure, D., Bonnifait, L., Kirstetter, P.E., 2014. Geostatistical radar-
618 raingauge merging: A novel method for the quantification of rain estimation accuracy. *Advances in*
619 *Water Resources* 71, 110–124. <https://doi.org/10.1016/j.advwatres.2014.06.005>
- 620 D’Odorico, P., Rigon, R., 2003. Hillslope and channel contributions to the hydrologic response. *Water*
621 *Resources Research* 39, 1–9. <https://doi.org/10.1029/2002WR001708>
- 622 Dolcine, L., Andrieu, H., Sempere-Torres, D., Creutin, D., 2001. Flash food forecasting with coupled
623 precipitation model in mountainous Mediterranean Basin. *Journal of Hydrologic Engineering* 6.
624 [https://doi.org/10.1061/\(ASCE\)1084-0699\(2001\)6:1\(1\)](https://doi.org/10.1061/(ASCE)1084-0699(2001)6:1(1))
- 625 Dooge, J.C.I., 1959. A General Theory of the Unit Hydrograph. *Journal of Geophysical Research* 64, 241–256.
- 626 Douinot, A., Roux, H., Garambois, P.A., Dartus, D., 2018. Using a multi-hypothesis framework to improve the
627 understanding of flow dynamics during flash floods. *Hydrology and Earth System Sciences* 22, 5317–
628 5340. <https://doi.org/10.5194/hess-22-5317-2018>
- 629 Duband, D., Obled, C., Rodriguez, J.Y., 1993. Unit hydrograph revisited: an alternate iterative approach to UH
630 and effective precipitation identification. *Journal of Hydrology* 150, 115–149.
631 [https://doi.org/10.1016/0022-1694\(93\)90158-6](https://doi.org/10.1016/0022-1694(93)90158-6)

632 Emmanuel, I., Andrieu, H., Leblois, E., Janey, N., Payrastra, O., 2015. Influence of rainfall spatial variability on
633 rainfall – runoff modelling : Benefit of a simulation approach ? *Journal of Hydrology* 531, 337–348.
634 <https://doi.org/10.1016/j.jhydrol.2015.04.058>

635 Emmanuel, I., Payrastra, O., Andrieu, H., Zuber, F., 2017. A method for assessing the influence of rainfall
636 spatial variability on hydrograph modeling. First case study in the Cevennes Region, southern France.
637 *Journal of Hydrology* 555. <https://doi.org/10.1016/j.jhydrol.2017.10.011>

638 Fatichi, S., Vivoni, E.R., Ogden, F.L., Ivanov, V.Y., Mirus, B., Gochis, D., Downer, C.W., Camporese, M.,
639 Davison, J.H., Ebel, B., Jones, N., Kim, J., Mascaro, G., Niswonger, R., Restrepo, P., Rigon, R., Shen,
640 C., Sulis, M., Tarboton, D., 2016. An overview of current applications, challenges, and future trends in
641 distributed process-based models in hydrology. *Journal of Hydrology* 537, 45–60.
642 <https://doi.org/10.1016/j.jhydrol.2016.03.026>

643 Fisher, C.K., Pan, M., Wood, E.F., 2020. Spatiotemporal assimilation-interpolation of discharge records through
644 inverse streamflow routing. *Hydrology and Earth System Sciences* 24, 293–305.
645 <https://doi.org/10.5194/hess-24-293-2020>

646 Goni, M., López, J.J., Gimena, F.N., 2019. Geomorphological instantaneous unit hydrograph model with
647 distributed rainfall. *Catena* 172, 40–53. <https://doi.org/10.1016/j.catena.2018.08.010>

648 Gupta, V.K., Waymire, E., Wang, C.T., 1980. A representation of an instantaneous unit hydrograph from
649 geomorphology. *Water Resources Research* 16, 855–862. <https://doi.org/10.1029/WR016i005p00855>

650 Hayami, S., 1951. On the propagation of Flood Waves. *Disaster Prevention Research Institute Bulletin* 1, 1–16.

651 Kirkby, M.J., 1976. Tests of the random network model, and its application to basin hydrology. *Earth Surface*
652 *Processes* 1, 197–212. <https://doi.org/10.1002/esp.3290010302>

653 Marani, A., Rigon, R., Rinaldo, A., 1991. A Note on Fractal Channel Networks. *Water Resources Research* 27,
654 3041–3049. <https://doi.org/10.1029/91WR02077>

655 McMillan, H., 2020. Linking hydrologic signatures to hydrologic processes: A review. *Hydrological Processes*
656 34, 1393–1409. <https://doi.org/10.1002/hyp.13632>

657 Menke, W., 2012. *Geophysical Data Analysis: Discrete Inverse Theory* MATLAB edition, Book.
658 <https://doi.org/10.1016/B978-0-12-397160-9.00001-1>

659 Moussa, R., 1997. Geomorphological transfer function calculated from digital elevation models for distributed
660 hydrological modelling. *Hydrological Processes* 11, 429–449. [https://doi.org/10.1002/\(SICI\)1099-1085\(199704\)11:5<429::AID-HYP471>3.0.CO;2-J](https://doi.org/10.1002/(SICI)1099-1085(199704)11:5<429::AID-HYP471>3.0.CO;2-J)

661

662 Moussa, R., Chahinian, N., Bocquillon, C., 2007. Distributed hydrological modelling of a Mediterranean
663 mountainous catchment – Model construction and multi-site validation. *Journal of Hydrology* 337, 35–
664 51. <https://doi.org/10.1016/j.jhydrol.2007.01.028>

665 Naulin, J.-P., Payrastra, O., Gaume, E., 2013. Spatially distributed flood forecasting in flash flood prone areas:
666 Application to road network supervision in Southern France. *Journal of Hydrology* 486, 88–99.
667 <https://doi.org/10.1016/j.jhydrol.2013.01.044>

668 Olivera, F., Maidment, D., 1999. Model for Runoff Routing. *Water Resources Research* 35, 1155–1164.
669 <https://doi.org/10.1029/1998WR900104>

670 Pan, M., Wood, E.F., 2013. Inverse streamflow routing. *Hydrology and Earth System Sciences* 17, 4577–4588.
671 <https://doi.org/10.5194/hess-17-4577-2013>

672 Rigon, R., Bancheri, M., Formetta, G., DeLavenne, A., 2016. The geomorphological unit hydrograph from a
673 historical-critical perspective. *Earth Surface Processes and Landforms* 41, 27–37.
674 <https://doi.org/10.1002/esp.3855>

675 Rinaldo, A., Marani, A., Rigon, R., 1991. Geomorphological Dispersion. *Water Resources Research* 27, 513–
676 525.

677 Rodriguez, F., Cudennec, C., Andrieu, H., 2005. Application of morphological approaches to determine unit
678 hydrographs of urban catchments. *Hydrological Processes* 19. <https://doi.org/10.1002/hyp.5643>

679 Rodriguez-Iturbe, I., Rinaldo, A., 1997. *Fractal River Basins: Chance and Self-Organization*, Cambridge
680 University Press. ed.

681 Rodriguez-Iturbe, I., Valdés, J.B., 1979. The geomorphologic structure of hydrologic response. *Water Resources*
682 *Research* 15, 1409–1420. <https://doi.org/10.1029/WR015i006p01409>

683 Ross, C.W., Prihodko, L., Anchang, J., Kumar, S., Ji, W., Hanan, N.P., 2018. Global Hydrologic Soil Groups
684 (HYSOGs250m) for Curve Number-Based Runoff Modeling.
685 <https://doi.org/10.3334/ORNLDAAC/1566>

686 Saco, P.M., Kumar, P., 2002a. Kinematic dispersion in stream networks 1. Coupling hydraulic and network
687 geometry. *Water Resources Research* 38, 26-1-26–14. <https://doi.org/10.1029/2001wr000695>

688 Saco, P.M., Kumar, P., 2002b. Kinematic dispersion in stream networks 2. Scale issues and self-similar network
689 organization. *Water Resources Research* 38, 27-1-27–15. <https://doi.org/10.1029/2001wr000694>

690 Saulnier, G.-M., Le Lay, M., 2009. Sensitivity of flash-flood simulations on the volume, the intensity, and the
691 localization of rainfall in the Cévennes-Vivarais region (France). *Water Resources Research* 45.
692 <https://doi.org/10.1029/2008WR006906>

693 Sherman, L.K., 1932. Stream flow from rainfall by the unit hydrograph method. *Engineering News Record* 501–
694 505.

695 Singh, P.K., Mishra, S.K., Jain, M.K., 2014. A review of the synthetic unit hydrograph: from the empirical UH
696 to advanced geomorphological methods. *Hydrological Sciences Journal* 59, 239–261.
697 <https://doi.org/10.1080/02626667.2013.870664>

698 Smith, J.A., Baeck, M.L., Meierdiercks, K.L., Nelson, P.A., Miller, A.J., Holland, E.J., 2005. Field studies of the
699 storm event hydrologic response in an urbanizing watershed. *Water Resources Research* 41.
700 <https://doi.org/10.1029/2004WR003712>

701 Smith, J.A., Baeck, M.L., Morrison, J.E., Sturdevant-Rees, P., Turner-Gillespie, D.F., Bates, P.D., 2002. The
702 Regional Hydrology of Extreme Floods in an Urbanizing Drainage Basin. *Journal of Hydrometeorology*
703 3, 267–282. [https://doi.org/10.1175/1525-7541\(2002\)003<0267:TRHOEF>2.0.CO;2](https://doi.org/10.1175/1525-7541(2002)003<0267:TRHOEF>2.0.CO;2)

704 Tarboton, D.G., 1997. A new method for the determination of flow directions and upslope areas in grid digital
705 elevation models. *Water Resources Research* 33, 309–319. <https://doi.org/10.1029/96WR03137>

706 Tarentola, A., 2005. *Inverse Problem Theory*, SIAM, Society for Industrial and Applied Mathematics. ed.
707 Philadelphia.

708 Trambly, Y., Bouvier, C., Ayral, P.A., Marchandise, A., 2011. Impact of rainfall spatial distribution on rainfall-
709 runoff modelling efficiency and initial soil moisture conditions estimation. *Natural Hazards and Earth*
710 *System Science* 11, 157–170. <https://doi.org/10.5194/nhess-11-157-2011>

- 711 Vannier, O., Anquetin, S., Braud, I., 2016. Investigating the role of geology in the hydrological response of
 712 Mediterranean catchments prone to flash-floods: Regional modelling study and process understanding.
 713 Journal of Hydrology 541, 158–172. <https://doi.org/10.1016/j.jhydrol.2016.04.001>
- 714 Volpi, E., Di Lazzaro, M., Fiori, A., 2012. A simplified framework for assessing the impact of rainfall spatial
 715 variability on the hydrologic response. Advances in Water Resources 46, 1–10.
 716 <https://doi.org/10.1016/j.advwatres.2012.04.011>
- 717 Wood, E.F., Sivapalan, M., Beven, K., 1990. Similarity and scale in catchment storm response. Reviews of
 718 Geophysics 28, 1–18. <https://doi.org/10.1029/RG028i001p00001>
- 719 Woods, R., Sivapalan, M., 1999. A synthesis of space-time variability in storm response: Rainfall, runoff
 720 generation, and routing. Water Resources Research 35, 2469–2485.
 721 <https://doi.org/10.1029/1999WR900014>
- 722 Yao, C., Zhang, K., Yu, Z., Li, Z., Li, Q., 2014. Improving the flood prediction capability of the Xinanjiang
 723 model in ungauged nested catchments by coupling it with the geomorphologic instantaneous unit
 724 hydrograph. Journal of Hydrology 517, 1035–1048. <https://doi.org/10.1016/j.jhydrol.2014.06.037>
- 725 Zeng, Z., Tang, G., Hong, Y., Zeng, C., Yang, Y., 2017. Development of an NRCS curve number global dataset
 726 using the latest geospatial remote sensing data for worldwide hydrologic applications. null 8, 528–536.
 727 <https://doi.org/10.1080/2150704X.2017.1297544>
- 728 Zoccatelli, D., Borga, M., Zanon, F., Antonescu, B., Stancalie, G., 2010. Which rainfall spatial information for
 729 flash flood response modelling? A numerical investigation based on data from the Carpathian range,
 730 Romania. Journal of Hydrology 394, 148–161. <https://doi.org/10.1016/j.jhydrol.2010.07.019>

732 **Appendix – Sensitivity study**

733 This sensitivity analysis has focused on the influence of the application conditions on the identified E-
 734 GIUHs. More specifically, it has concerned: the confidence assigned to flow data (coefficient of variation α_Q),
 735 the confidence assigned to the GIUH theoretical model (coefficients of variation α_E and α_V), the influence of the
 736 *a priori* value of D_{E0} , the influence of the *a priori* value of U_{E0} , and lastly the influence of this error on the *a*
 737 *priori* net hyetograph.

738 This study has been performed by running the E-GIUH identification method while varying one of these
 739 factors with respect to the reference conditions. The influence was then assessed by calculating: i) the mean
 740 Nash efficiency criterion between the observed and resulting hydrographs (NSE_Q), ii) the mean Nash efficiency
 741 criterion between the resulting E-GIUHs and the reference E-GIUH (NSE_{GIUH}), and iii) the mean absolute
 742 deviation between the series of reference values of U_E and D_E , respectively. The results of this sensitivity
 743 analysis are displayed in Figure 8 and lead to the following conclusions:

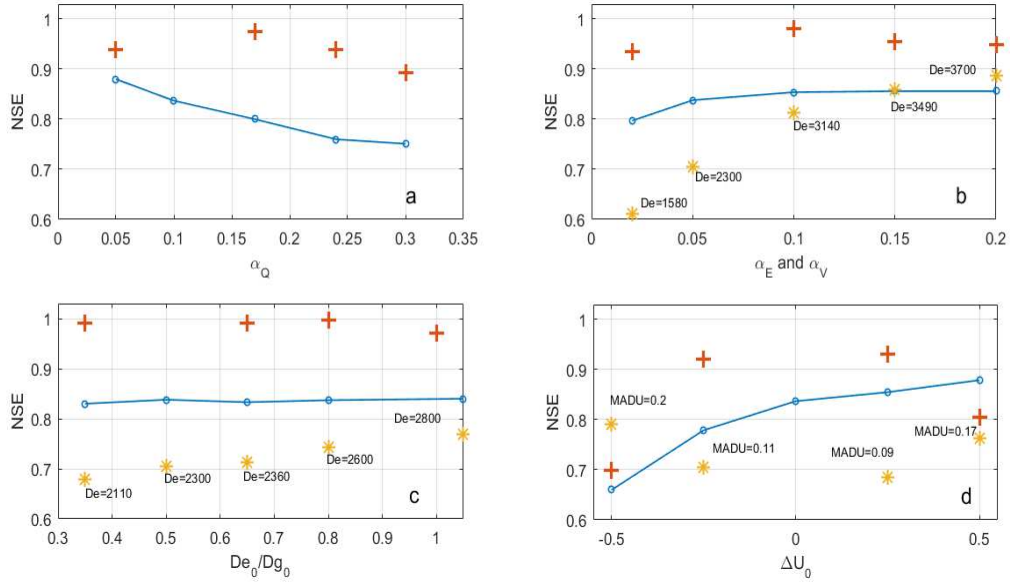
744 - *Confidence assigned to flow data (Fig. A1-a)*: The increase in the coefficient of variation α_Q , which reflects
 745 a loss of confidence in the measured flow data, clearly yields a reduced quality of the resulting hydrographs
 746 (blue line). The value of NSE_{GIUH} remains above 0.94, which denotes a moderate influence on the identified E-

747 GIUH with respect to the reference one, except for $\alpha_Q = 0.3$, where the E-GIUH change is more pronounced
748 ($NSE_{GIUH} = 0.89$).

749 - *Confidence assigned to the GIUH model (Fig. A1-b)*: A very strong confidence in GIUH theory ($\alpha_E = \alpha_V =$
750 0.02) results in a lower quality of the obtained hydrographs. This quality improves and stabilizes quickly at
751 $NSE_Q \approx 0.85-0.86$ as α_E and α_V increase. The value of NSE_{GIUH} is higher than 0.95 when α_E and $\alpha_V \geq 0.05$,
752 which denotes a weak influence on the identified E- GIUH with respect to the reference one. The more
753 noteworthy effect pertains to the mean identified value of D_E , which rises from $1560 \text{ m}^2\text{s}^{-1}$ to $3700 \text{ m}^2\text{s}^{-1}$, at
754 which point the constraints on GIUH theory are relaxed without the quality criteria being significantly modified.
755 This finding confirms that the identification of D_E is far from being straightforward based on the available
756 observations.

757 - *Influence of the a priori value of D_{E0} (Fig. A1-c)*: The *a priori* value of D_{E0} has been increased from
758 $0.35 D_{G0}$ to D_{G0} . The influence of this value appears to be very weak, while the values of NSE_Q and NSE_{GIUH}
759 remain nearly constant at respectively $0.83-0.84$ and 0.99 . The mean identified value of D_E increases from
760 $2110 \text{ m}^2\text{s}^{-1}$ to $2800 \text{ m}^2\text{s}^{-1}$ with respect to D_{E0} ; this influence is less marked than that for α_E and α_V .

761 - *Influence of the a priori value of U_{E0} (Fig. A1-d)*: This influence is tested by defining the *a priori*
762 value $U_{E0} = U_E^* + \Delta U$, with U_E^* being the solution obtained according to the reference application conditions,
763 and $\Delta U = [-0.5, 0.25, 0.0, 0.25, 0.5] \text{ (m/s)}$. Note that a modification of U_{E0} also de facto affects D_{E0} . The
764 results obtained indicate that: i) a strong underestimation of U_E^* ($\Delta U = -0.5 \text{ m/s}$) cannot be corrected by the
765 identification procedure ($NSE_Q = 0.66, NSE_{GIUH} = 0.7$ and $MAD_U = 0.2 \text{ m/s}$); ii) the situation is more
766 satisfactory for a moderate underestimation or overestimation ($\Delta U = \pm 0.25 \text{ m/s}$), for which the final GIUHs do
767 not differ substantially from the reference solutions ($NSE_{GIUH} = 0.92$ and 0.93 and $MAD_U =$
768 0.11 and 0.09 m/s , respectively), and iii) an initial overestimation of velocity by the *a priori* value appears to be
769 less detrimental than an underestimation.



770

771 Figure A1: Sensitivity study of the E-GIUH identification: (A) influence of α_Q , (B) : influence of α_E and α_V ,
 772 (C) : influence of the *a priori* value D_{E0} ; (D) : Influence of the *a priori* celerity U_{E0}
 773 NSE_Q (blue line), NSE_{GIUH} (red crosses),

774

775 - Influence of this error covariance on the *a priori* net hyetograph.

776 The E-GIUH identification has been performed by varying the value of α_R from $\alpha_R = 0.03$ (excellent
 777 confidence in the *a priori* net hyetograph) to $\alpha_R = 0.30$ (weak confidence). These results are illustrated in Figure
 778 A2, in its display of the evolution in NSE_Q between the observed hydrographs and the hydrographs simulated
 779 using the final set of parameters, in offering the following insights:

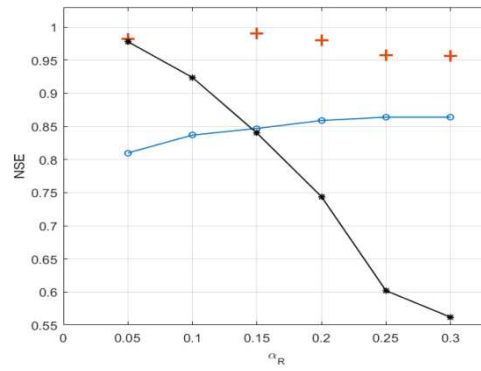
780 - The increase of α_R results in an increase of NSE_Q , which rises from $NSE_Q = 0.83$ for $\alpha_R = 0.03$ to $NSE_Q =$
 781 0.88 for $\alpha_R = 0.24$, meaning that the set of parameters characterizing basin operations ($\overline{R}_n, EGIUH$) is globally
 782 better determined.

783 - This improvement is not correlated with significant changes in the identified E-GIUHs, which do not differ
 784 significantly from the E-GIUH reference application conditions. Indeed, the value of NSE_{GIUH} remains above
 785 0.97 for $\alpha_R = 0.17$ and $\alpha_R = 0.24$.

786 - This improvement is mainly derived from changes in the resulting net hyetographs, in comparison with the *a*
 787 *priori* net hyetographs, as confirmed by the value of NSE_{Rn} calculated between the *a priori* and identified net
 788 hyetographs, which decreases from 0.99 to 0.55 as α_R increases from 0.05 to 0.3 .

789 This sensitivity analysis has confirmed that relaxing the constraint on the *a priori* net hyetograph yields an
 790 overall more efficient functioning of the identification algorithm, which leads to a coupled identification of the

791 $(\overline{R_n}, EGIUH)$ couple without modifying the resulting E-GIUH by considering the *a priori* net hystograph to be
792 accurate.



793

794 Figure A2 : Sensitivity study of the E-GIUH identification to the application conditions : influence of α_R

795 NSE_Q (blue line), NSE_{GIUH} (red crosses), NSE_{Rn} (black line)

796